

Phonon and crystal field excitations in geometrically frustrated rare earth titanates

T.T.A. Lummen,¹ I.P. Handayani,¹ M.C. Donker,¹ D. Fausti,¹ G. Dhalenne,² P. Berthet,² A. Revcolevschi,² and P.H.M. van Loosdrecht^{1,*}

¹*Zernike Institute for Advanced Materials, University of Groningen, Nijenborgh 4, 9747 AG Groningen, The Netherlands*

²*Laboratoire de Physico-Chimie de l'Etat Solide, CNRS, UMR8182, Université Paris-Sud, Bâtiment 414, 91405 Orsay, France*

(Dated: May 29, 2018)

The phonon and crystal field excitations in several rare earth titanate pyrochlores are investigated. Magnetic measurements on single crystals of $\text{Gd}_2\text{Ti}_2\text{O}_7$, $\text{Tb}_2\text{Ti}_2\text{O}_7$, $\text{Dy}_2\text{Ti}_2\text{O}_7$ and $\text{Ho}_2\text{Ti}_2\text{O}_7$ are used for characterization, while Raman spectroscopy and terahertz time domain spectroscopy are employed to probe the excitations of the materials. The lattice excitations are found to be analogous across the compounds over the whole temperature range investigated (295-4 K). The resulting full phononic characterization of the $\text{R}_2\text{Ti}_2\text{O}_7$ pyrochlore structure is then used to identify crystal field excitations observed in the materials. Several crystal field excitations have been observed in $\text{Tb}_2\text{Ti}_2\text{O}_7$ in Raman spectroscopy for the first time, among which all of the previously reported excitations. The presence of additional crystal field excitations, however, suggests the presence of two inequivalent Tb^{3+} sites in the low temperature structure. Furthermore, the crystal field level at approximately 13 cm^{-1} is found to be both Raman and dipole active, indicating broken inversion symmetry in the system and thus undermining its current symmetry interpretation. In addition, evidence is found for a significant crystal field-phonon coupling in $\text{Tb}_2\text{Ti}_2\text{O}_7$. These findings call for a careful reassessment of the low temperature structure of $\text{Tb}_2\text{Ti}_2\text{O}_7$, which may serve to improve its theoretical understanding.

PACS numbers: 63.20.dd, 71.70.Ch, 75.50.Lk, 75.30.Cr

I. INTRODUCTION

The term 'geometrical frustration'^{1,2,3} applies to a system, when it is unable to simultaneously minimize all of its magnetic exchange interactions, solely due to its geometry. Magnetically interacting spins residing on such lattices are unable to order into a unique magnetic ground state due to the competing magnetic interactions between different lattice sites. Instead of selecting a single, unique magnetic ground state at low temperatures, a pure magnetically frustrated system has a macroscopically degenerate ground state. In real systems however, any secondary, smaller term (arising from single-ion or exchange anisotropy, further neighbor interactions, dipolar interactions, small lattice distortions or a magnetic field, for example) in the system's Hamiltonian can favor certain magnetic ground states at very low temperatures, thereby (partially) lifting this peculiar degeneracy. In this fact lies the origin of the vast richness and diversity of the low temperature magnetic behavior of different frustrated systems in nature^{1,4,5,6,7}.

Geometries suitable to exhibit frustration typically consist of infinite networks of triangles or tetrahedra, which share one or more lattice sites. One of the most common structures known to be able to induce magnetic frustration is that of the pyrochlores, $\text{A}_2\text{B}_2\text{O}_7$, where both the A^{3+} ions (rare earth element, coordinated to 8 O atoms) and the B^{4+} ions (transition metal element, coordinated to 6 O atoms) reside on a lattice of corner-sharing tetrahedra, known as the pyrochlore lattice. Thus, if either A^{3+} or B^{4+} is a magnetic species,

frustration may occur due to competing interactions. A subclass of the pyrochlores is formed by the rare earth titanate family, $\text{R}_2\text{Ti}_2\text{O}_7$, where the R^{3+} ion is the only (para-)magnetic species, since Ti^{4+} is diamagnetic ($3d^0$). For the pyrochlore lattice, both theory^{8,9,10} and Monte Carlo simulations^{10,11} predict a 'collective paramagnetic' ground state, or the lack of long range magnetic ordering, for classical Heisenberg spins at finite temperature. The quantum Heisenberg spin ($S = 1/2$) model for the pyrochlore lattice also predicts a quantum disordered system at finite temperatures, a state often referred to as a 'spin liquid'¹². However, in reality the different perturbative terms in the corresponding Hamiltonian result in quite diverse low temperature magnetic behavior among the different rare earth titanates⁴, of which the Gd, Tb, Ho and Dy variants are studied here.

The supposedly least complex case is that of gadolinium titanate, $\text{Gd}_2\text{Ti}_2\text{O}_7$. The Gd^{3+} ion has, in contrast to the Tb^{3+} , Ho^{3+} and Dy^{3+} ions, a spin only $^8S_{7/2}$ ($L = 0$) ground state, rendering the influence of crystal field levels and possible induced Ising-like anisotropy insignificant in $\text{Gd}_2\text{Ti}_2\text{O}_7$. The experimentally determined Curie-Weiss temperature of $\text{Gd}_2\text{Ti}_2\text{O}_7$ is $\simeq -10 \text{ K}$ ^{13,14,15}, indicating antiferromagnetic nearest neighbor interactions. Thus, $\text{Gd}_2\text{Ti}_2\text{O}_7$ could be considered as an ideal realization of the frustrated Heisenberg antiferromagnet with dipolar interactions. Experimentally, $\text{Gd}_2\text{Ti}_2\text{O}_7$ has been found to undergo a magnetic ordering transition at $\simeq 1 \text{ K}$ ¹³. However, this transition corresponds to only partial ordering of the magnetic structure, as only 3 spins per tetrahedron order¹⁶. In this

partially ordered state the spins residing on the [111] planes of the crystal (which can be viewed as Kagomé planes) are ordered in a 120° configuration, parallel to the Kagomé plane, while the spins residing on the interstitial sites remain either statically or dynamically disordered¹⁷. Subsequent experimental investigations revealed a second ordering transition at $\simeq 0.7$ K, corresponding to the partial ordering of the interstitial disordered spins^{15,17} which, however, do remain (partially) dynamic down to 20mK.^{18,19} Despite of $\text{Gd}_2\text{Ti}_2\text{O}_7$ supposedly being well approximated by the Heisenberg antiferromagnet with dipolar interactions, theoretical justification for this complex magnetic behavior remains difficult^{13,18,20}.

In $\text{Tb}_2\text{Ti}_2\text{O}_7$, the dominant interactions are antiferromagnetic, as indicated by the experimentally determined Curie-Weiss temperature, $\theta_{CW} \simeq -19$ K²¹. A study of the diluted compound $(\text{Tb}_{0.02}\text{Y}_{0.98})_2\text{Ti}_2\text{O}_7$ revealed that the contribution to θ_{CW} due to exchange and dipolar interactions is $\simeq -13$ K, comparable to the θ_{CW} -value found in $\text{Gd}_2\text{Ti}_2\text{O}_7$ ²². Despite the energy scale of these interactions, the Tb^{3+} moments do not show long range magnetic order down to as low as 50 mK, making it the system closest to a real 3D *spin liquid* to date^{21,23}. However, crystal field (CF) calculations indicate a ground state doublet and Ising-like easy axis anisotropy for the (7F_6) Tb^{3+} magnetic moments along their local $\langle 111 \rangle$ directions (the direction towards the center of the tetrahedron the particular atom is in), which would dramatically reduce the degree of frustration in the system^{22,24,25,26,27}. Theoretical models taking this anisotropy into account predict magnetic ordering temperatures of about 1 K^{22,28}. Subsequent theoretical work suggests that the magnetic moment anisotropy is more isotropic than Ising-like, which could suppress magnetic ordering²⁹. Recently, $\text{Tb}_2\text{Ti}_2\text{O}_7$ was argued to be in a quantum mechanically fluctuating 'spin ice' state^{30,31}. Virtual quantum mechanical CF excitations (the first excited CF doublet is separated by only $\simeq 13$ cm^{-1} from the ground state doublet^{22,25,27}) are proposed to rescale the effective theoretical model from the unfrustrated Ising antiferromagnet to a frustrated *resonating spin ice* model. Nevertheless, the experimentally observed lack of magnetic ordering down to the millikelvin range and the true magnetic ground state in $\text{Tb}_2\text{Ti}_2\text{O}_7$ remain as of yet enigmatic^{31,32,33,34}.

Illustrating the diversity in magnetic behavior due to the subtle differences in the rare earth species of the titanates, the situation in both $\text{Dy}_2\text{Ti}_2\text{O}_7$ ^{35,36,37} and $\text{Ho}_2\text{Ti}_2\text{O}_7$ ^{38,39,40,41} is again different. The R^{3+} ions in these compounds have a ${}^6H_{15/2}$ (Dy^{3+}) and a 5I_8 (Ho^{3+}) ground state, respectively, with corresponding free ion magnetic moments $\mu = 10.65 \mu_B$ (Dy^{3+}) and $\mu = 10.61 \mu_B$ (Ho^{3+}). These systems were first thought to have weak ferromagnetic nearest neighbor exchange interactions, as indicated by the small positive values of θ_{CW} , $\simeq 2$ K and $\simeq 1$ K for $\text{Dy}_2\text{Ti}_2\text{O}_7$ and $\text{Ho}_2\text{Ti}_2\text{O}_7$, respectively⁴². More recently, however, the nearest neighbor *exchange* interactions in $\text{Dy}_2\text{Ti}_2\text{O}_7$ and

$\text{Ho}_2\text{Ti}_2\text{O}_7$ were argued to be *antiferromagnetic*⁴³. The effective ferromagnetic interaction between the spins in fact is shown to be due to the dominant ferromagnetic long-range magnetic dipole-dipole interactions^{28,44}. The R^{3+} -ions in both $\text{Dy}_2\text{Ti}_2\text{O}_7$ and $\text{Ho}_2\text{Ti}_2\text{O}_7$ are well described by a well separated Ising doublet (first excited states are at ~ 266 and ~ 165 cm^{-1} , respectively²⁴) with a strong single ion anisotropy along the local $\langle 111 \rangle$ directions. Unlike for antiferromagnetically interacting spins with local $\langle 111 \rangle$ Ising anisotropy, *ferromagnetically* interacting Ising spins on a pyrochlore lattice should be highly frustrated^{38,45}. As Anderson already pointed out half a century ago⁴⁶, the resulting model is analogous to Pauling's ice model⁴⁷, which earned both $\text{Dy}_2\text{Ti}_2\text{O}_7$ and $\text{Ho}_2\text{Ti}_2\text{O}_7$ the title of 'spin ice' compound^{38,44,45,48}. Although numerical simulations predict long range order at low temperatures for this model⁴³, experimental studies report no transition to a long range ordered state for either $\text{Dy}_2\text{Ti}_2\text{O}_7$ ^{28,35,49,50} or $\text{Ho}_2\text{Ti}_2\text{O}_7$ ^{38,51,52}, down to as low as 50 mK.

As is apparent from above considerations, the low temperature magnetic behavior of the rare earth titanates is dictated by the smallest of details in the structure and interactions of the material. Therefore, a comprehensive experimental study of the structural, crystal field and magnetic properties of these systems may serve to clarify unanswered questions in their understanding. In this paper, dc magnetic susceptibility measurements, polarized Raman scattering experiments and terahertz time domain spectroscopy on aforementioned members of the rare earth titanates family are employed to gain more insight into the details that drive them towards such diverse behavior. Raman scattering allows for simultaneous investigation of structural and crystal field (CF) properties through the observation of both phononic and CF excitations, while the comparison between the various members helps identify the nature of the different excitations observed.

II. EXPERIMENTAL

A. Sample Preparation

Polycrystalline samples of $\text{R}_2\text{Ti}_2\text{O}_7$ (where $\text{R} = \text{Gd}, \text{Tb}, \text{Dy}, \text{Ho}$) were synthesized by firing stoichiometric amounts of high purity ($> 99.9\%$) TiO_2 and the appropriate rare earth oxide (Gd_2O_3 , Tb_4O_7 , Dy_2O_3 or Ho_2O_3 , respectively), in air, for several days with intermittent grindings. The resulting polycrystalline powder was subsequently prepared for single crystal growth, using the method described by Gardner, Gaulin and Paul⁵³. The following single crystal growth (also done as described in ref. 49) using the floating zone technique yielded large, high quality single crystals of all of the $\text{R}_2\text{Ti}_2\text{O}_7$ variants. Discs ($\simeq 1$ mm thickness) with a,b-plane surfaces were cut from oriented single crystals and subsequently polished, in order to optimize scattering experiments. The

Tb₂Ti₂O₇ sample used in Raman experiments was subsequently polished down to $\simeq 250 \mu\text{m}$ thickness to facilitate THz transmission measurements.

B. Instrumentation

X-ray Laue diffraction, using a Philips PW 1710 diffractometer equipped with a Polariod XR-7 system, was employed to orient the single crystal samples of Gd₂Ti₂O₇ and Tb₂Ti₂O₇ for the polarized Raman spectroscopy experiments, while simultaneously confirming the single crystallinity of the samples. The Dy₂Ti₂O₇ and Ho₂Ti₂O₇ single crystals were oriented using an Enraf Nonius CAD4 diffractometer.

The magnetic susceptibilities of the obtained rare earth titanates were measured using the Quantum Design MPMS-5 SQUID magnetometer of the 'Laboratoire de Physico-Chimie de l'Etat Solide' (LPCES), CNRS, UMR8182 at the 'Université Paris-Sud in Orsay, France. The R₂Ti₂O₇ samples, about 100 mg of single crystal (in the form of discs of approximately 4 mm diameter and 1 mm thickness), were placed in cylindrical plastic tubes and locked in position. Next, the samples were zero-field-cooled down to 1.7 K, after which the magnetization of the sample was measured as a function of the temperature in an applied magnetic field of 100 Oe, while warming the sample.

Polarization controlled, inelastic light scattering experiments were performed on all oriented R₂Ti₂O₇ samples. The experiments were performed in a 180° backscattering configuration, using a triple grating micro-Raman spectrometer (T64000 Jobin-Yvon), consisting of a double grating monochromator (acting as a spectral filter) and a polychromator which disperses the scattered light onto a liquid nitrogen cooled CCD detector. The frequency resolution was better than 2 cm^{-1} for the frequency region considered. The samples were placed in a liquid helium cooled optical flow-cryostat (Oxford Instruments). The temperature was stabilized with an accuracy of 0.1 K in the whole range of measured temperatures (from 2.5 to 295 K). The 532.6 nm (frequency doubled) output of a Nd:YVO₄ laser was focused on the Gd₂Ti₂O₇, Tb₂Ti₂O₇ and Dy₂Ti₂O₇ samples using a 50x microscope objective and used as excitation source in the scattering experiments. A Krypton laser (676.4 nm) was used as the excitation source for the scattering experiments on the Ho₂Ti₂O₇ sample, since 532.6 nm excitation (resonant at low temperatures in case of Ho₂Ti₂O₇) results in fluorescence dominating the inelastic scattering spectrum in the 5-800 cm^{-1} spectral range. The power density on the samples was of the order of $50 \mu\text{W}/\mu\text{m}^2$ in all cases. The polarization was controlled both on the incoming and outgoing beam. Parallel (\parallel) and perpendicular (\perp) measurements on Gd₂Ti₂O₇ and Tb₂Ti₂O₇ were performed along crystallographic axes of the a,b surface of the samples, Porto notations c(aa)c and c(ab)c, respectively. Unfortunately, the orientation of the a and

b axes in the (a,b) plane of the Dy₂Ti₂O₇ and Ho₂Ti₂O₇ surfaces with respect to the light polarizations was not known. Analogous Porto notations are c(xx)c (\parallel) and c(xy)c (\perp), respectively, where x is a direction in the (a,b) plane of the sample making an undetermined angle α with the a axis, while y, in the same a,b plane of the crystal, is perpendicular to the x direction. Raman spectra were fitted with lorentzian lineshapes to extract mode parameters.

Terahertz time domain spectroscopy (THz TDS)⁵⁴ was performed on Tb₂Ti₂O₇ using a home made setup similar to those described elsewhere^{54,55}. THz pulses (pulse duration of several ps, frequency range 0.3-2.5 THz) were generated through a difference frequency generation process in a ZnTe single crystal upon pulsed excitation (120 fs, 800 nm) by an amplified Ti:sapphire system. The magnitude of the time dependent electric field transmitted through the sample (w.r.t. that transmitted through vacuum) was measured at various temperatures, through electro-optic sampling in a second ZnTe single crystal, using 800 nm pulses of approximately 120 fs. The sample used was a thin slice of single crystalline Tb₂Ti₂O₇ (the same sample as used in the Raman experiments), which was mounted on a copper plate with an aperture ($\varnothing 2 \text{ mm}$) and placed in a liquid helium cooled optical flow-cryostat (Oxford Instruments). The polarization of the THz radiation was parallel to the crystallographic a-axis.

III. RESULTS AND DISCUSSION

A. Magnetic Measurements

The magnetic susceptibility χ , defined as the ratio of the magnetization of the sample to the applied magnetic field, of all the rare earth titanate samples was measured in a 100 Oe applied magnetic field. Since the samples used were plate-like discs, the data have been corrected by a demagnetization factor as calculated for flat, cylindrical plates⁵⁶. Fig. 1 shows the inverse molar susceptibilities of all samples in the low temperature regime. For each sample, the data was fitted to a Curie-Weiss form for the molar magnetic susceptibility of an antiferromagnet:

$$\chi_m = \frac{2C}{(T - \theta)} + B, \quad (1)$$

where C is the Curie constant in CGS units ($C = N_A \mu^2 \mu_B^2 / 3k_b \simeq \mu^2 / 8$, in [$\text{emu} \cdot \text{K} \cdot \text{mol}^{-1}$]), θ is the expected transition temperature (giving an indication of the sign of the magnetic interactions) and B is a temperature independent Van Vleck contribution to the susceptibility. The model was fitted to high temperature experimental data (100 K and up, where the demagnetization correction is of the order of 1 %) and linear regression analysis of $\chi_{m,i}^{-1}$ yielded the experimental values for θ_i , μ_i and B_i . These are tabulated below in table 1, together with several values reported in literature.

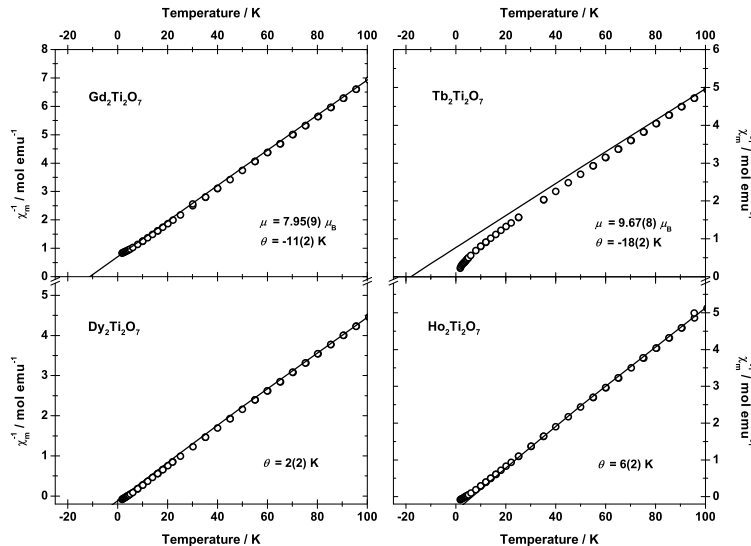


FIG. 1: Inverse molar magnetic susceptibilities (open circles) of all $R_2Ti_2O_7$ samples and their corresponding Curie-Weiss fits (solid lines, eq. 1) versus temperature. The Curie-Weiss law, which is fitted to the higher temperature data (> 100 K) is obeyed down to low temperatures.

TABLE I: Experimentally determined and literature values for θ_i , μ_i and B_i for the different $R_2Ti_2O_7$ compounds. The numbers in between brackets give the accuracy in the last decimal of the values.

Compound i (source)	θ_i (K)	μ_i (μ_B)	B_i ($emu \cdot mol^{-1}$)
Gd ₂ Ti ₂ O ₇ (exp.)	-11(2)	7.95(9)	0 ^a
Gd ₂ Ti ₂ O ₇ (lit.) ¹³	-9,6	7.7	-
Gd ₂ Ti ₂ O ₇ (lit.) ¹⁴	-11,7	7.8	-
Gd ₂ Ti ₂ O ₇ (lit.) ⁴²	-8,95(6)	7.224(3)	$6.0 \cdot 10^{-4}$
Tb ₂ Ti ₂ O ₇ (exp.)	-18(2)	9.67(7)	$3.4(9) \cdot 10^{-3}$
Tb ₂ Ti ₂ O ₇ (lit.) ^{21,22}	-19	9.6	-
Dy ₂ Ti ₂ O ₇ (exp.)	2(2)	- ^b	- ^b
Dy ₂ Ti ₂ O ₇ (lit.) ⁴²	$\simeq 1,0$	9.590(6)	$1.1(1) \cdot 10^{-2}$
Ho ₂ Ti ₂ O ₇ (exp.)	6(2)	- ^b	- ^b
Ho ₂ Ti ₂ O ₇ (lit.) ⁴²	$\simeq 2,0$	9.15(3)	$1.2(1) \cdot 10^{-2}$

^aWhen fitting χ_m with a nonzero B term, it becomes negligibly small. The best fit is obtained with $B=0$.

^bSince dipolar interactions are dominant in this case, no reliable values were extracted (see text).

In general, the experimentally obtained data compare (where possible) favorable to the various values reported in literature (table I). The extracted θ parameters for Dy₂Ti₂O₇ and Ho₂Ti₂O₇ do slightly deviate from literature values, presumably due to the estimation of the demagnetization factor (fits to the present uncorrected data yield θ values of approximately 1 and 2 K, respectively). The experimentally determined paramagnetic moments obtained for Gd₂Ti₂O₇ and Tb₂Ti₂O₇ are also in excellent agreement with the corresponding free ion values, which are $\mu = 7.94 \mu_B$ and $\mu = 9.72 \mu_B$ for the Gd³⁺

(⁸ $S_{7/2}$) and Tb³⁺ (⁷ F_6) free ions, respectively. The large negative Curie-Weiss temperatures for Gd₂Ti₂O₇ and Tb₂Ti₂O₇ indicate antiferromagnetic exchange coupling. In contrast, the small, positive θ values for Ho₂Ti₂O₇ and Dy₂Ti₂O₇ initially led to the assumption of weak ferromagnetic exchange interactions between nearest neighbor Dy³⁺ and Ho³⁺ ions⁴². As stated above, however, since the Ho³⁺ and Dy³⁺ ions have a large magnetic moment (free ion values are $\mu = 10.607 \mu_B$ (⁵ I_8 ground state) and $\mu = 10.646 \mu_B$ (⁶ $H_{15/2}$ ground state), respectively), the dipolar interactions between neighboring R³⁺ ions are dominating the effective nearest neighbor (n.n.) interactions. The n.n. *exchange* interactions are in fact *antiferromagnetic*⁴³, while the dominant dipolar n.n. interactions are of ferromagnetic nature^{28,44}. Consequently, the effective n.n. interactions are slightly ferromagnetic, resulting in the positive θ values. Another consequence of the dipolar interactions and being dominant is the fact that extracting the real values of μ and B from the inverse susceptibility curves becomes non-trivial, since more elaborate models taking the dipolar interaction into account are needed.

B. Raman Spectroscopy

1. Room temperature spectra

To determine the Raman active vibrations of the single crystals, group theory analysis was employed. This predicts that, for the cubic rare earth titanate structure (R₂Ti₂O₇) of space group $Fd\bar{3}m$ (O_h^7), the sublattices

of the unit cell span the following irreducible representations:

$$\begin{aligned}
 16(c)\text{-site: Ti}^{4+} - \text{sublattice} &= A_{2u} + E_u + 2F_{1u} + F_{2u} \\
 16(d)\text{-site: R}^{3+} - \text{sublattice} &= A_{2u} + E_u + 2F_{1u} + F_{2u} \\
 48(f)\text{-site: O}(1) - \text{sublattice} &= A_{1g} + E_g + 2F_{1g} + 3F_{2g} + \\
 &\quad A_{2u} + E_u + 3F_{1u} + 2F_{2u} \\
 8(a)\text{-site: O}(2) - \text{sublattice} &= F_{1u} + F_{2g}
 \end{aligned}$$

This makes the following decomposition into zone center normal modes (excluding the F_{1u} acoustic mode):

$$\Gamma = A_{1g} + E_g + 2F_{1g} + 4F_{2g} + 3A_{2u} + 3E_u + 7F_{1u} + 4F_{2u}$$

Of these normal modes, only the A_{1g} , E_g and the 4 F_{2g} modes are Raman active. The 7 F_{1u} modes are infrared active and the remaining modes are optically inactive. The symmetry coordinates for the optically active normal modes are given by Gupta *et al.*⁵⁷. Based on the symmetries of the Raman active modes, the A_{1g} and E_g modes are expected to be observed in parallel polarization (\parallel) spectra, while the F_{2g} modes are expected in the perpendicular polarization (\perp) spectra. Surprisingly, the room temperature spectra of $R_2Ti_2O_7$ show all the Raman active modes in both polarizations. Angle dependent Raman measurements (varying the angle between the incoming light polarization and the b-axis from -45° to 45°) reveal no orientation in which the theoretical selection rules are fully obeyed. Polycrystallinity and/or crystalline disorder is however, not believed to be the cause, since other techniques (X-ray Laue diffraction, magnetic measurements) reveal no such signs. Also, to our best knowledge, no Raman spectrum of any of these rare earth titanates fulfilling their phononic selection rules has been published. Although no full compliance of phononic selection rules was observed, the nature of the Raman active modes was clearly identified, through their angular dependence. Their assignment is indicated in fig. 2 as well as in table II. The figure depicts the room temperature (RT), parallel polarization spectra of the rare earth titanates and the corresponding modes. The assignment of the mode symmetries is based on comparison with assignments in previous works on these^{57,58,59,60,61,62} and related^{62,63,64,65,66,67} compounds (see table II), on aforementioned measurements (not shown) of the angular dependence of mode intensities and on the temperature dependence of the modes (*vide infra*).

Comparison between the RT Raman spectra yields the conclusion that the nature of the R^{3+} ion has only slight influence on the Raman active vibrational modes. This is not surprising, since in all the Raman active modes only the oxygen atoms are displaced^{57,58}. Consequently, there is no obvious systematic variation of the phonon frequencies with the mass of the respective rare earth ions, as has been noted before for the rare earth titanates⁵⁷, hafnates⁶⁶, manganates⁶³ and stannates⁶⁵. The assignment of the $R_2Ti_2O_7$ modes in literature has been mostly consistent (see Table II), yet there are a few debated details. There is general agreement on the nature of the

modes at $\simeq 210 \text{ cm}^{-1}$ (F_{2g} , O(2)-sublattice mode⁵⁸), $\simeq 519 \text{ cm}^{-1}$ (A_{1g} , R-O stretching mode^{59,60}) and $\simeq 556 \text{ cm}^{-1}$ (F_{2g} , O(1)-sublattice mode⁵⁸). Temperature and angle dependent Raman measurements show the band around $\simeq 315 \text{ cm}^{-1}$ to consist of two modes, a F_{2g} mode around 310 cm^{-1} (O-R-O bending mode^{59,60}) and an E_g mode around 327 cm^{-1} (O(1)-sublattice mode⁵⁸), as recognized by Saha *et al.*⁵⁸ and Vandenborre *et al.*⁶⁷. Earlier works either interchanged the mode assignment within this band^{57,59} or ascribed the whole band to only one of these modes^{60,61}. However, our temperature and angle dependent measurements confirm the assignment made by Saha *et al.* The last expected phonon, an F_{2g} mode, has been either not accounted for⁵⁷, combined with the A_{1g} mode in one band^{58,62} or ascribed to low intensity peaks around 105^{60} , 450^{59} or 680^{61} cm^{-1} in previous works. Here, it is ascribed to a broad, low intensity mode around $\simeq 260 \text{ cm}^{-1}$. This mode is not clearly resolved in the RT spectra due to the fact that it overlaps largely with the neighboring, strong F_{2g} modes at $\simeq 210 \text{ cm}^{-1}$ and $\simeq 309 \text{ cm}^{-1}$. Fitting with those two peaks only, however, does not adequately reproduce the experimental spectral shape in the the $200\text{-}300 \text{ cm}^{-1}$ window. Additionally, as the temperature is lowered, the phonon modes sharpen and the existence of this excitation becomes obvious in the spectra. Worth noting are also the two anomalous modes in $Tb_2Ti_2O_7$ at $\simeq 303$ (F_{2g}) and $\simeq 313 \text{ cm}^{-1}$ (E_g), which have lower frequencies and wider lineshapes compared to their counterparts in the other, isostructural rare earth titanates.

Next to the expected Raman active vibrations, the spectra in this work show some very weak scattering intensity at low wavenumbers (first two rows in table II), which has been reported before^{60,62}. Vandenborre *et al.*⁶² were unable to account for this intensity in their calculations, while Mori *et al.*⁶⁰ offer the plausible assignment to trace R_2O_3 in the system. The latter assignment is also tentatively adopted here. Mori *et al.* also suggested the 'missing' F_{2g} mode may be responsible for some of this low wavenumber intensity. Additionally, a weak mode is observed at 450 cm^{-1} in most $R_2Ti_2O_7$ compounds, as was also seen before. Zhang *et al.*⁵⁹ and Hess *et al.*⁶¹ ascribed the 'missing' F_{2g} mode to this feature. Alternatively, Mori *et al.*⁶⁰ interpreted it as being due to trace amounts of starting compound TiO_2 , which is known⁶⁸ to have a phonon at 447 cm^{-1} . The true origin of this mode is at present unclear. Finally, there is some low intensity scattering intensity at higher wavenumbers, around 700 cm^{-1} (last two rows of table II). This intensity has been observed before^{58,59,60,61,62} and is ascribed to forbidden IR modes made active by slight, local non-stoichiometry in the system.^{58,60}

2. Temperature dependence

Raman spectra of the $R_2Ti_2O_7$ crystals were recorded at temperatures ranging from RT to 4 K. Figure 3 depicts

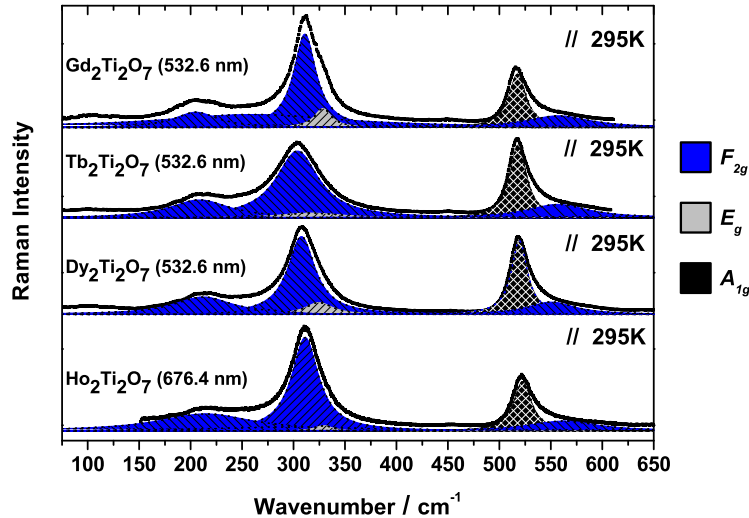


FIG. 2: (Color online) Room temperature Raman spectra of the $R_2Ti_2O_7$ crystals in parallel polarization configuration. The assignment of the Raman active modes to the observed peaks is indicated by the colored lorentzian lineshapes.

the evolution of both the parallel (\parallel) and perpendicular (\perp) polarization Raman spectra of the $R_2Ti_2O_7$ crystals with decreasing temperature.

Going down in temperature several spectral changes occur in the Raman spectra. The evolution of the phononic excitations with temperature are very similar in the different $R_2Ti_2O_7$ lattices. Again, this is not surprising, since only oxygen atoms are displaced in the Raman active phonons^{57,58}. Firstly, the lowest frequency phonon (F_{2g} , $\omega \simeq 210 \text{ cm}^{-1}$ at RT) shows a strong softening ($\omega \simeq 170 \text{ cm}^{-1}$ at 4 K) and sharpening with decreasing temperature, revealing the previously unresolved F_{2g} mode ($\omega_{RT} \simeq 260 \text{ cm}^{-1}$), which also softens ($\omega_{4K} \simeq 190 \text{ cm}^{-1}$), but doesn't show a strong narrowing. Secondly, the sharpening of both the $\simeq 309 \text{ cm}^{-1}$ F_{2g} and the $\simeq 324 \text{ cm}^{-1}$ E_g mode decreases their spectral overlap, clearly justifying the two-mode interpretation of the $\simeq 315 \text{ cm}^{-1}$ band at RT. Additionally, both modes show a slight softening upon cooldown. Also the A_{1g} phonon ($\omega_{RT} \simeq 519 \text{ cm}^{-1}$) shows the familiar softening ($\omega_{4K} \simeq 511 \text{ cm}^{-1}$) and sharpening trend on cooling. Finally, due to its large width and low intensity, describing the temperature evolution of the highest frequency F_{2g} phonon proves rather difficult, though it seems to soften slightly. Comparison of the $R_2Ti_2O_7$ spectra in fig. 3 yields the observation that the anomalous phonons (at $\simeq 303$ (F_{2g}) and $\simeq 313 \text{ cm}^{-1}$ (E_g)) in $Tb_2Ti_2O_7$ remain wide throughout the temperature range, in contrast to the corresponding modes in the other titanates. Additionally, these modes are shifting in opposite directions in $Tb_2Ti_2O_7$ only: the F_{2g} mode softens ($\omega_{4K} \simeq 295 \text{ cm}^{-1}$) while the E_g mode considerably hardens ($\omega_{4K} \simeq 335 \text{ cm}^{-1}$). An explanation for this anomalous behavior could be coupling of

these phonons to low frequency crystal field excitations of the Tb^{3+} -ions (vide infra).

3. Crystal field excitations

Aside from the phonons in the Raman spectra of $R_2Ti_2O_7$, several spectra also show crystal field (CF) excitations of the R^{3+} ions at low temperatures, as shown in fig. 4. The CF level splitting in the different rare earth ions depends on their electronic configuration and their local surroundings. In the $R_2Ti_2O_7$ family, the simplest case is that of the Gd^{3+} ion ($4f^7$), which has a spin only $^8S_{7/2}$ ($L = 0$) ground state, resulting in the absence of a level splitting due to the local crystal field. Consequently, the Raman spectrum of $Gd_2Ti_2O_7$ shows no CF excitations, making it a suitable 'template' of the $R_2Ti_2O_7$ Raman spectrum with lattice excitations only. Combined with the strong correspondence of the phononic excitations in the $R_2Ti_2O_7$ spectra, it allows for quick identification of CF modes in the other compounds.

More complicated is the CF level splitting in the Tb^{3+} ion ($4f^8$), which has a 7F_6 ground state. Several studies calculating the crystal field for the Tb^{3+} -ion in $Tb_2Ti_2O_7$ ^{22,25,26,27}, based on inelastic neutron scattering results^{21,22,25,27,69,70}, yielded slightly differing energy level schemes for the lowest crystal field levels of Tb^{3+} in $Tb_2Ti_2O_7$ as is schematically depicted in fig. 5. Here, solid lines depict CF levels observed experimentally, while dotted lines indicate CF levels obtained through CF calculations. Shown in fig. 6, which is a zoom-in on the low-wavenumber region of the 4 K perpendicular polarization spectrum of $Tb_2Ti_2O_7$, are the

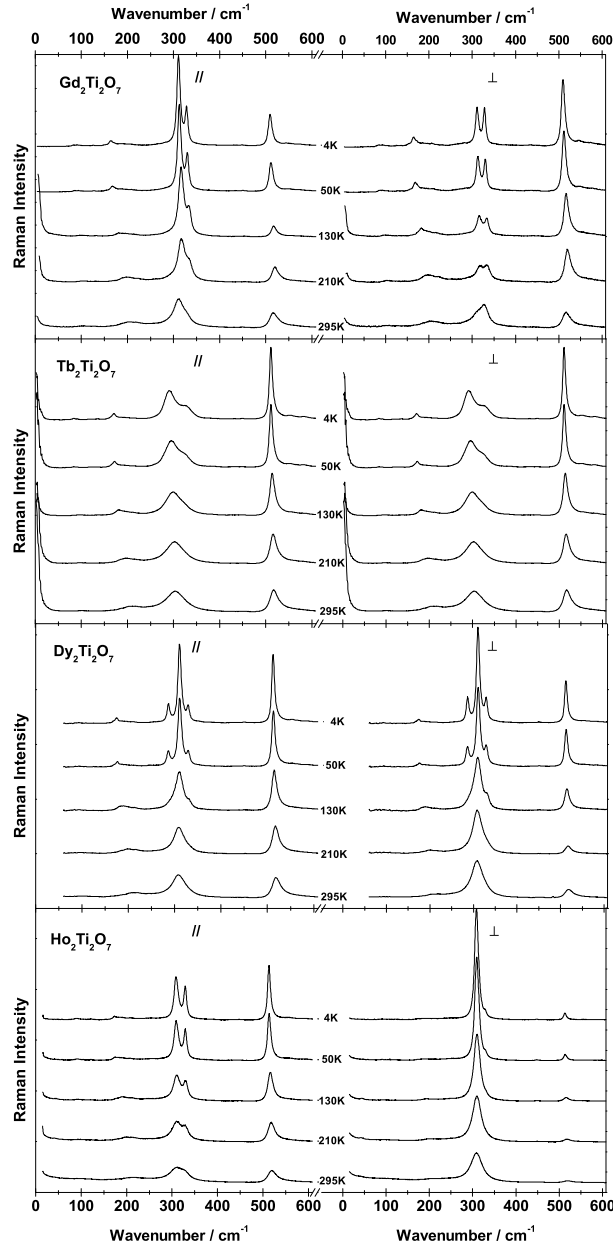


FIG. 3: Temperature dependence of the $R_2Ti_2O_7$ parallel (\parallel) and perpendicular (\perp) Raman spectra. The spectra show several changes when going down in temperature (see text), most of which (the phononic excitations) are analogous for all $R_2Ti_2O_7$ lattices. In addition, at lower temperatures various crystal field excitations appear in the spectra of some of the rare earth titanates (See fig. 4). Spectra are normalized to the integrated intensity of the depicted frequency window.

CF excitations that are observed using inelastic light scattering. As is also clear from fig. 5, all CF excitations previously observed using inelastic neutron scattering are also observed here. Furthermore, additional low-lying excitations can be seen, which are easily identified as CF levels, by comparison with the 'lattice-only

template' spectrum of $Gd_2Ti_2O_7$.

The excitations from the crystal field ground state to the higher crystal field levels, of approximate calculated values 13, 60, 83 and 118 cm^{-1} (see fig. 5), are all observed at very similar frequencies, at 12.9, 60.8, 83.1 and 119.2 cm^{-1} , respectively. The 60.8 cm^{-1} level has not

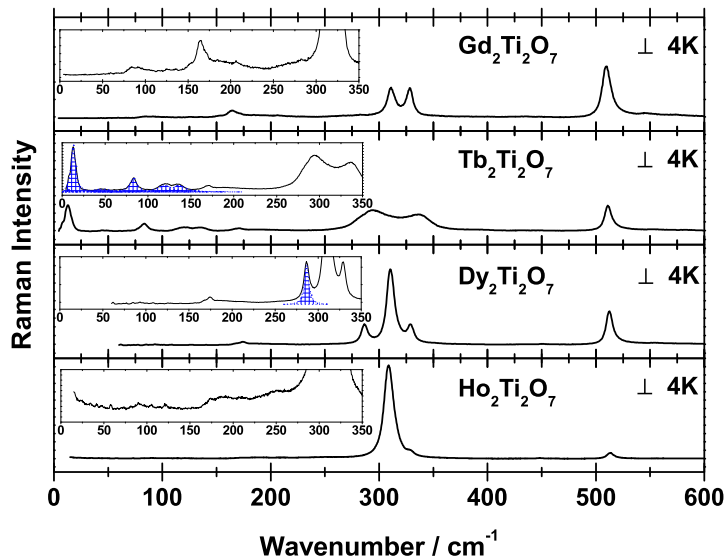


FIG. 4: (Color online) Low temperature spectra for all $R_2Ti_2O_7$ as measured in perpendicular polarization configuration. The spectra are normalized on the total integrated intensity of the spectra. The insets show respective zoom-ins on the lower wavenumber regions of the spectra, where the excitations identified as CF levels of the rare earth ions are indicated by dotted blue lorentzian peaks. $Gd_2Ti_2O_7$ shows only phononic modes and can be regarded as the lattice template. $Tb_2Ti_2O_7$ and $Dy_2Ti_2O_7$ show additional CF modes, while $Ho_2Ti_2O_7$ shows again only lattice excitations. A fitted lorentzian centered at zero (Rayleigh line) is subtracted from the $Tb_2Ti_2O_7$ data for clarity.

been observed experimentally before, though it did follow from the CF calculation made by Gingras *et al.*²². Conversely, the $\approx 135.2 \text{ cm}^{-1}$ mode has been observed through inelastic neutron scattering, yet has not been accounted for in CF calculations. Although Gardner *et al.*²⁷ interpreted it as an optical phonon, this excitation is clearly identified as a CF excitation here, through the isostructural comparison with the other titanates. The latter assignment is also made by Mirebeau *et al.*²⁵. Additionally, new CF excitations are observed at 7.7 and 47.2 cm^{-1} . While the former is recognized as a CF excitation from the CF ground state to a new CF energy level, the 47.2 cm^{-1} could also be interpreted as an excitation from the excited CF level at 12.9 cm^{-1} to the higher excited CF level at 60.8 cm^{-1} . While such an excitation is Raman active (see below), its occurrence at 4 K seems unlikely, since at this temperature the excited CF level (12.9 $\text{cm}^{-1} \approx 19 \text{ K}$) is not expected to be populated enough to give rise to a measurable Raman signal. Additionally, were it an excitation from an excited state, its intensity would decrease upon cooling. Instead, the intensity of this mode steadily increases with decreasing temperature.

Using E_g and E_g , A_{2g} and A_{1g} irreducible representations^{22,26} for the ground state and excited CF levels, respectively, it can be confirmed that indeed all these ground state to excited state transitions are ex-

pected to be Raman active. Through analogous considerations, the lowest excitation ($E_g \rightarrow E_g$, 13 cm^{-1}) is found to be symmetry forbidden in a direct dipole transition. In this respect, terahertz time domain spectroscopy (THz TDS) in the range of 10 to 50 cm^{-1} (0.3 to 1.5 THz) was employed to probe the absorption of $Tb_2Ti_2O_7$ at various temperatures. Using this technique it is possible to extract complex optical quantities in the THz range through the direct measurement of the time trace of the transmitted THz pulse. The obtained curves for the real ($\epsilon_1(\nu)$) and imaginary ($\epsilon_2(\nu)$) parts of the dielectric constant at various temperatures are plotted in fig. 7. The plots clearly show an absorption around 0.45 THz (15 cm^{-1}) at low temperatures, corresponding to the 13 cm^{-1} CF level also observed in the Raman spectra of $Tb_2Ti_2O_7$. This is corroborated by the identical temperature dependence of the mode in both methods: its spectral signature decreases with increasing temperature, vanishing around 90 K. The fact that the 13 cm^{-1} CF level is observed in a direct dipole transition indicates that this level is not a true $E_g \rightarrow E_g$ transition, since such a dipole transition would be symmetry forbidden.

Overall, the existence of the additional CF levels in $Tb_2Ti_2O_7$ unaccounted for by CF calculations, suggests the presence of a second Tb^{3+} site in the structure, with an energy level scheme different from those reported previously. Three additional CF levels are observed exper-

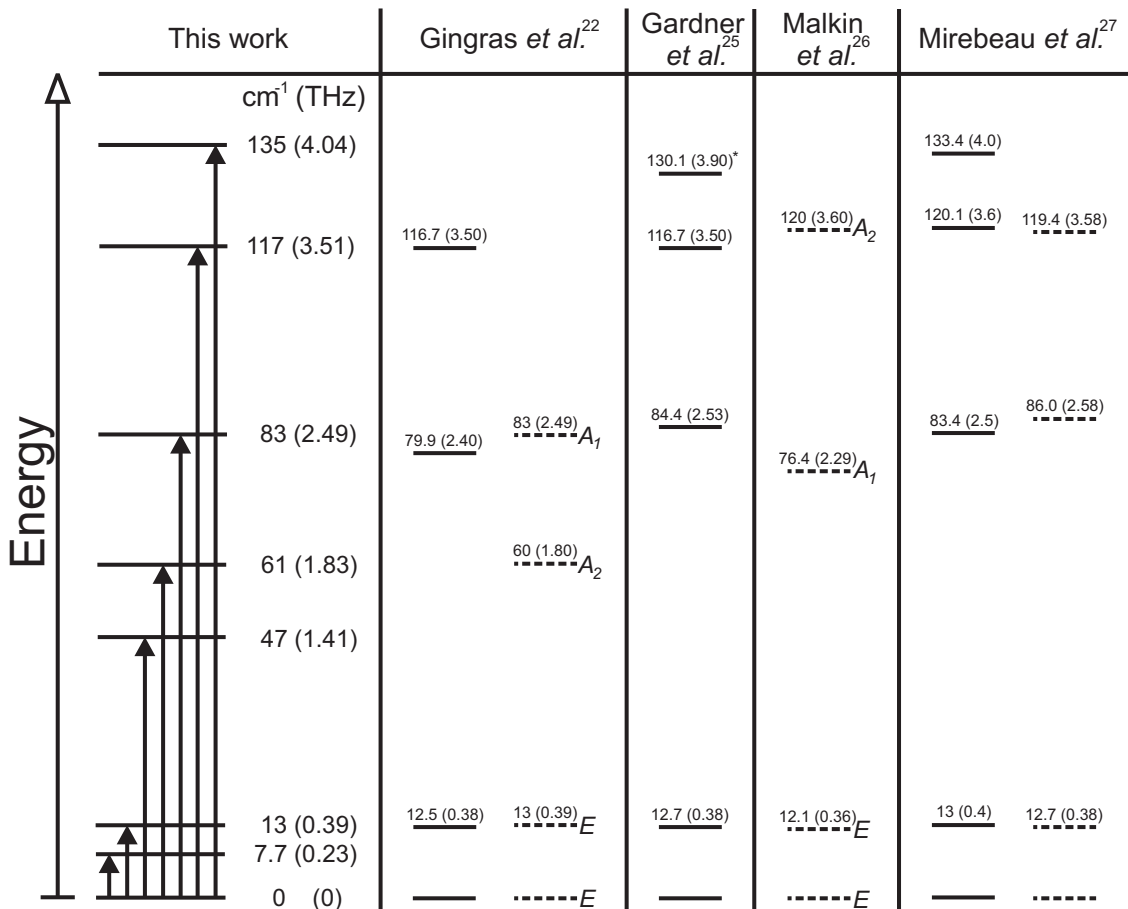


FIG. 5: Various CF energy level schemes of the Tb^{3+} ion in $\text{Tb}_2\text{Ti}_2\text{O}_7$. Solid lines depict CF levels that have been observed experimentally, while dotted lines represent CF levels as calculated using CF calculations. Numbers indicate CF level energies in cm^{-1} (THz) and symbols in italics indicate symmetries of corresponding levels. Solid arrows indicate all CF excitations observed in the low temperature Raman spectrum of $\text{Tb}_2\text{Ti}_2\text{O}_7$ (see fig. 6).

imentally, while four would naively be expected for a slightly differing Tb site in this low wavenumber region. A fourth new CF level might be unresolved due to the strong CF level at 83 cm^{-1} or might simply be symmetry forbidden in a Raman transition. Moreover, the fact that the $\sim 13 \text{ cm}^{-1}$ CF level is simultaneously Raman and dipole active indicates the breaking of inversion symmetry in the system, which questions the validity of its current symmetry interpretation. Recently, the exact symmetry of the $\text{Tb}_2\text{Ti}_2\text{O}_7$ lattice has been extensively studied. Han *et al.*⁷¹ performed neutron powder diffraction and x-ray absorption fine-structure experiments down to 4.5 K, revealing a perfect pyrochlore lattice, within experimental error. Ofer *et al.*⁷² find no static lattice distortions on the timescale of $0.1 \mu\text{s}$, down to 70 mK. Most recently, however, Ruff *et al.*⁷³ found finite structural correlations at temperatures below 20 K, indicative of fluctuations above a very low temperature structural transition. The present experimental results suggest these fluctuations may even induce a minute static disorder, resulting in the observed CF level diagram.

In $\text{Dy}_2\text{Ti}_2\text{O}_7$ the Dy^{3+} ions ($4f^9$) have a ${}^6H_{15/2}$ ground

state. Crystal field calculations have been performed by Jana *et al.*⁷⁴, who deduced an energy level scheme consisting of eight Kramers' doublets, with a separation of $\simeq 100 \text{ cm}^{-1}$ of the first excited state. Malkin *et al.*²⁶ and Rosenkranz *et al.*⁷⁵ estimated the first excited state gap to be $> 200 \text{ cm}^{-1}$ and $\simeq 266 \text{ cm}^{-1}$, respectively. The Raman spectrum of $\text{Dy}_2\text{Ti}_2\text{O}_7$ shows only one extra excitation compared to the 'lattice template' spectrum of $\text{Gd}_2\text{Ti}_2\text{O}_7$, at an energy of $\sim 287 \text{ cm}^{-1}$. This excitation is tentatively ascribed to the first excited CF level, comparing most favorably to the estimation of Rosenkranz *et al.*

For $\text{Ho}_2\text{Ti}_2\text{O}_7$, ground state 5I_8 ($\text{Ho}^{3+}, 4f^{10}$), several CF energy level schemes have been calculated^{26,75,76,77}, all with first excited state separations around 150 cm^{-1} . However, the Raman spectrum of $\text{Ho}_2\text{Ti}_2\text{O}_7$ does not show any clear inelastic light scattering from CF levels to compare these calculations to. Although there is some weak intensity around $\simeq 150 \text{ cm}^{-1}$, which compares favorably with all of the calculated level schemes, the intensity of this scattering is insufficient to definitively ascribe it to a CF level.

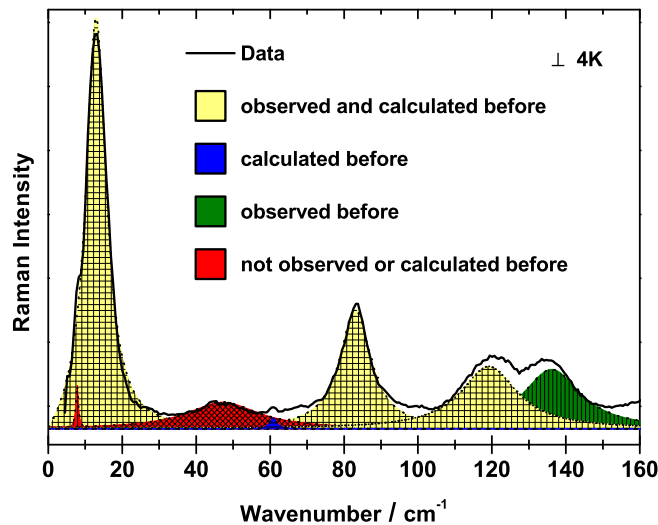


FIG. 6: (Color online) The low wavenumber region of the perpendicular polarization Raman spectrum of $\text{Tb}_2\text{Ti}_2\text{O}_7$ at 4 K. A fitted lorentzian centered at zero (Rayleigh line) is subtracted from the data for clarity. The crystal field levels (see fig. 5) are indicated by the filled lorentzian lineshapes that were fit to the data. A distinction has been made between CF levels that have been calculated and observed before (yellow), CF levels that have been calculated before, but so far have not been observed (blue), CF levels that have been observed before, but have not been calculated (green) and additional CF levels that are observed for the first time using inelastic light scattering (red).

IV. CONCLUSIONS

To summarize, several members of the rare earth titanates family $\text{R}_2\text{Ti}_2\text{O}_7$ were studied using magnetic susceptibility measurements and polarized inelastic light scattering experiments. Lattice excitations were found to vary only slightly between crystals with different rare earth ions. Temperature dependent measurements also revealed completely analogous behavior of the phononic excitations, except for two anomalous phonons in $\text{Tb}_2\text{Ti}_2\text{O}_7$, which seem to be coupled to the low energy crystal field excitations in that compound. Such crystal field excitations were observed in $\text{Tb}_2\text{Ti}_2\text{O}_7$ and possibly also in $\text{Dy}_2\text{Ti}_2\text{O}_7$. Only one non-phononic excitation is clearly observed in $\text{Dy}_2\text{Ti}_2\text{O}_7$, its energy consistent with estimates of the first excited crystal field level. For $\text{Tb}_2\text{Ti}_2\text{O}_7$, all of the the previously determined crystal field energy levels were confirmed. Moreover, the resulting energy level diagram was expanded by three newly observed CF levels, only one of which has been calculated before. Also, one previously reported level was found to

be both Raman and dipole active, contradicting its current presumed symmetry. These findings may reflect the existence of two inequivalent Tb sites in the low temperature structure or a static symmetry reduction of another nature, suggesting the recently found structural correlations to induce a minute static disorder in $\text{Tb}_2\text{Ti}_2\text{O}_7$ at very low temperatures. The new crystal field information may serve to help elucidate the complex theoretical enigma of $\text{Tb}_2\text{Ti}_2\text{O}_7$.

Acknowledgments

The authors would like to thank F. van der Horst for his help using the PW 1710 diffractometer. We also acknowledge fruitful discussions with M. Mostovoi, D. Khomskii and S. Singh. This work is part of the research programme of the 'Stichting voor Fundamenteel Onderzoek der Materie (FOM)', which is financially supported by the 'Nederlandse Organisatie voor Wetenschappelijk Onderzoek (NWO)'

* Electronic address: P.H.M.van.Loosdrecht@rug.nl

¹ A. P. Ramirez, *Annu. Rev. Mater. Sci.* **24**, 453 (1994).

² P. Schiffer and A. P. Ramirez, *Comments Condens. Matter Phys.* **18**, 21 (1996).

³ H. T. Diep, ed., *Magnetic Systems with Competing Interactions* (World Scientific, Singapore, 1994).

⁴ J. E. Greedan, *J. Alloys Compd.* **408-412**, 444 (2006).

⁵ J. E. Greedan, *J. Mater. Chem.* **11**, 37 (2001).

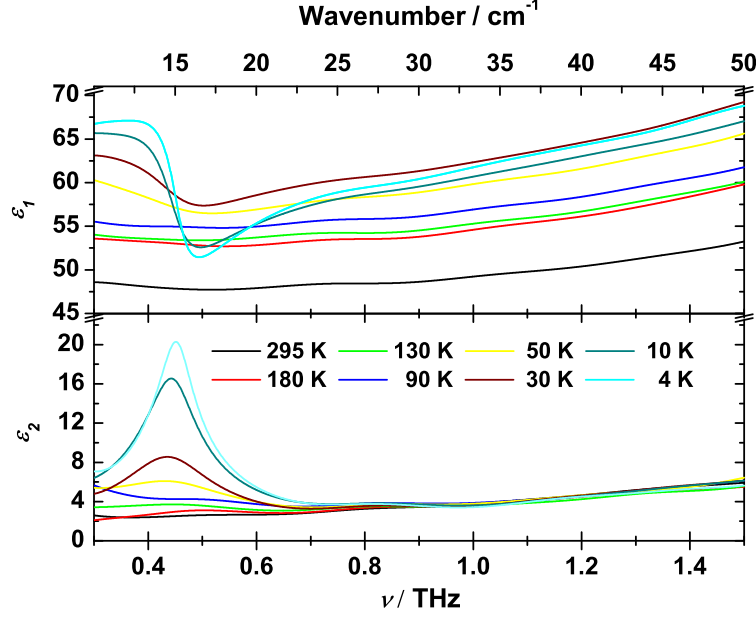


FIG. 7: (Color online) Real (upper panel) and imaginary (lower panel) parts of the complex dielectric constant of $\text{Tb}_2\text{Ti}_2\text{O}_7$ in the THz regime. The color legend holds for both panels.

- ⁶ M. F. Collins and O. A. Petrenko, *Can. J. Phys.* **75**, 605 (1997).
- ⁷ R. Moessner, *Can. J. Phys.* **79**, 1283 (2001).
- ⁸ J. Villain, *Z. Phys. B* **33**, 31 (1979).
- ⁹ J. N. Reimers, A. J. Berlinsky, and A. C. Shi, *Phys. Rev. B* **43**, 865 (1991).
- ¹⁰ R. Moessner and J. T. Chalker, *Phys. Rev. Lett.* **80**, 2929 (1998).
- ¹¹ J. N. Reimers, *Phys. Rev. B* **45**, 7287 (1992).
- ¹² B. Canals and C. Lacroix, *Phys. Rev. Lett.* **80**, 2933 (1998).
- ¹³ N. P. Raju, M. Dion, M. J. P. Gingras, T. E. Mason, and J. E. Greedan, *Phys. Rev. B* **59**, 14489 (1999).
- ¹⁴ J. D. Cashion, A. H. Cooke, M. J. M. Leask, T. L. Thorp, and M. R. Wells, *J. Mater. Sci.* **3**, 402 (1968).
- ¹⁵ A. P. Ramirez, B. S. Shastry, A. Hayashi, J. J. Krajewski, D. A. Huse, and R. J. Cava, *Phys. Rev. Lett.* **89**, 067202 (2002).
- ¹⁶ J. D. M. Champion, A. S. Wills, T. Fennell, S. T. Bramwell, J. S. Gardner, and M. A. Green, *Phys. Rev. B* **64**, 140407(R) (2001).
- ¹⁷ J. R. Stewart, G. Ehlers, A. S. Wills, S. T. Bramwell, and J. S. Gardner, *J. Phys.: Condens. Matter* **16**, L321 (2004).
- ¹⁸ A. Yaouanc, P. Dalmas de Réotier, V. Glazkov, C. Marin, P. Bonville, J. A. Hodges, P. C. M. Gubbens, S. Sakarya, and C. Baines, *Phys. Rev. Lett.* **95**, 047203 (2005).
- ¹⁹ S. R. Dunsiger, R. F. Kiefl, J. A. Chakhalian, J. E. Greedan, W. A. MacFarlane, R. I. Miller, G. D. Morris, A. N. Price, N. P. Raju, and J. E. Sonier, *Phys. Rev. B* **73**, 172418 (2006).
- ²⁰ S. E. Palmer and J. T. Chalker, *Phys. Rev. B* **62**, 488 (2000).
- ²¹ J. S. Gardner, S. R. Dunsiger, B. D. Gaulin, M. J. P. Gingras, J. E. Greedan, R. F. Kiefl, M. D. Lumsden, W. A. MacFarlane, N. P. Raju, J. E. Sonier, et al., *Phys. Rev. Lett.* **82**, 1012 (1999).
- ²² M. J. P. Gingras, B. C. den Hertog, M. Faucher, J. S. Gardner, S. R. Dunsiger, L. J. Chang, B. D. Gaulin, N. P. Raju, and J. E. Greedan, *Phys. Rev. B* **62**, 6496 (2000).
- ²³ J. S. Gardner, A. Keren, G. Ehlers, C. Stock, E. Segal, J. M. Roper, B. Fåk, M. B. Stone, P. R. Hammar, D. H. Reich, et al., *Phys. Rev. B* **68**, 180401(R) (2003).
- ²⁴ S. Rosenkranz, A. P. Ramirez, A. Hayashi, R. J. Cava, R. Siddharthan, and B. S. Shastry, *J. Appl. Phys.* **87**, 5914 (2000).
- ²⁵ I. Mirebeau, P. Bonville, and M. Hennion, *Phys. Rev. B* **76**, 184436 (2007).
- ²⁶ B. Z. Malkin, A. R. Zakirov, M. N. Popova, S. A. Klimin, E. P. Chukalina, E. Antic-Fidancev, P. Goldner, P. Aschehoug, and G. Dhalenne, *Phys. Rev. B* **70**, 075112 (2004).
- ²⁷ J. S. Gardner, B. D. Gaulin, A. J. Berlinsky, P. Waldron, S. R. Dunsiger, N. P. Raju, and J. E. Greedan, *Phys. Rev. B* **64**, 224416 (2001).
- ²⁸ B. C. den Hertog and M. J. P. Gingras, *Phys. Rev. Lett.* **84**, 3430 (2000).
- ²⁹ Y. J. Kao, M. Enjalran, A. Del Maestro, H. R. Molavian, and M. J. P. Gingras, *Phys. Rev. B* **68**, 172407 (2003).
- ³⁰ The ground state configuration of the spin ice model is formed by satisfying conditions analogous to Pauling's 'ice rules': every tetrahedron has both two spins pointing into and two spins pointing out of the tetrahedron. This (under)constraint on the system again results in a macroscopically large number of degenerate ground states.
- ³¹ H. R. Molavian, M. J. P. Gingras, and B. Canals, *Phys. Rev. Lett.* **98**, 157204 (2007).

- ³² M. Enjalran, M. J. P. Gingras, Y. J. Kao, A. del Maestro, and H. R. Molavian, *J. Phys.: Condens. Matter* **16**, S673 (2004).
- ³³ G. Ehlers, A. L. Cornelius, T. Fennell, M. Koza, S. T. Bramwell, and J. S. Gardner, *Physica B* **385-386**, 307 (2004).
- ³⁴ S. H. Curnoe, *Phys. Rev. B* **75**, 212404 (2007).
- ³⁵ A. P. Ramirez, A. Hayashi, R. J. Cava, R. Siddharthan, and B. S. Shastry, *Nature* **399**, 333 (1999).
- ³⁶ J. Snyder, B. G. Ueland, J. S. Slusky, H. Karunadasa, R. J. Cava, and P. Schiffer, *Phys. Rev. B* **69**, 064414 (2004).
- ³⁷ A. P. Ramirez, C. L. Broholm, R. J. Cava, and G. R. Kowach, *Physica B* **280**, 290 (2000).
- ³⁸ M. J. Harris, S. T. Bramwell, D. F. McMorrow, T. Zeiske, and K. W. Godfrey, *Phys. Rev. Lett.* **79**, 2554 (1997).
- ³⁹ S. T. Bramwell, M. J. Harris, B. C. den Hertog, M. J. P. Gingras, J. S. Gardner, D. F. McMorrow, A. R. Wildes, A. L. Cornelius, J. D. M. Champion, R. G. Melko, et al., *Phys. Rev. Lett.* **87**, 047205 (2001).
- ⁴⁰ A. L. Cornelius and J. S. Gardner, *Phys. Rev. B* **64**, 060406(R) (2001).
- ⁴¹ O. A. Petrenko, M. R. Lees, and G. Balakrishnan, *Phys. Rev. B* **68**, 012406 (2003).
- ⁴² S. T. Bramwell, M. N. Field, M. J. Harris, and I. P. Parkin, *J. Phys.: Condens. Matter* **12**, 483 (2000).
- ⁴³ R. G. Melko and M. J. P. Gingras, *J. Phys.: Condens. Matter* **16**, R1277 (2004).
- ⁴⁴ S. T. Bramwell and M. J. P. Gingras, *Science* **294**, 1495 (2001).
- ⁴⁵ S. T. Bramwell and M. J. Harris, *J. Phys.: Condens. Matter* **10**, L215 (1998).
- ⁴⁶ P. W. Anderson, *Phys. Rev.* **102**, 1008 (1956).
- ⁴⁷ L. Pauling, *J. Am. Chem. Soc.* **57**, 2680 (1935).
- ⁴⁸ S. V. Isakov, R. Moessner, and S. L. Sondhi, *Phys. Rev. Lett.* **95**, 217201 (2005).
- ⁴⁹ H. Fukazawa, R. G. Melko, R. Higashinaka, Y. Maeno, and M. J. P. Gingras, *Phys. Rev. B* **65**, 054410 (2002).
- ⁵⁰ T. Fennell, O. A. Petrenko, G. Balakrishnan, S. T. Bramwell, J. D. M. Champion, B. Fak, M. J. Harris, and D. M. Paul, *Appl. Phys. A* **74**, S889 (2002).
- ⁵¹ M. J. Harris, S. T. Bramwell, T. Zeiske, D. F. McMorrow, and P. J. C. King, *J. of Mag. and Magn. Mater.* **177**, 757 (1998).
- ⁵² I. Mirebeau, A. Apetrei, I. N. Goncharenko, and R. Moessner, *J. Phys.: Condens. Matter* **16**, S635 (2006).
- ⁵³ J. S. Gardner, B. D. Gaulin, and D. M. Paul, *J. Crystal Growth* **191**, 740 (1998), and references therein.
- ⁵⁴ C. A. Schmuttenmaer, *Chem. Rev.* **62**, 1759 (2004).
- ⁵⁵ M. C. Beard, G. M. Turner, and C. A. Schmuttenmaer, *Phys. Rev. B* **62**, 15764 (2000).
- ⁵⁶ M. Sato and Y. Ishii, *J. Appl. Phys.* **66**, 983 (1989).
- ⁵⁷ H. C. Gupta, S. Brown, N. Rani, and V. B. Gohel, *J. Raman Spectrosc.* **32**, 41 (2001).
- ⁵⁸ S. Saha, D. V. S. Muthu, C. Pascanut, N. Dragoe, R. Suryanarayanan, G. Dhalenne, A. Revcolevschi, S. Karmakar, S. M. Sharma, and A. K. Sood, *Phys. Rev. B* **74**, 064109 (2006).
- ⁵⁹ F. X. Zhang and S. K. Saxena, *Chem. Phys. Lett.* **413**, 248 (2005).
- ⁶⁰ M. Mori, G. M. Tompsett, N. M. Sammes, E. Suda, and Y. Takeda, *Solid State Ionics* **158**, 79 (2003), and references therein.
- ⁶¹ N. J. Hess, B. D. Begg, S. D. Conradson, D. E. McCready, P. L. Gassman, and W. J. Weber, *J. Phys Chem. B* **106**, 4663 (2002).
- ⁶² M. T. Vandenborre and E. Husson, *J. Solid State Chem.* **50**, 362 (1983).
- ⁶³ S. Brown, H. C. Gupta, J. A. Alonso, and M. J. Martinez-Lope, *J. Raman Spectrosc.* **34**, 240 (2003).
- ⁶⁴ M. Glerup, O. F. Nielsen, and W. F. Poulsen, *J. Solid State Chem.* **160**, 25 (2001).
- ⁶⁵ H. C. Gupta, S. Brown, N. Rani, and V. B. Gohel, *Int. J. Inorg. Mater.* **3**, 983 (2001).
- ⁶⁶ H. C. Gupta, S. Brown, N. Rani, and V. B. Gohel, *J. Phys. Chem. Solids* **63**, 535 (2002).
- ⁶⁷ M. T. Vandenborre, E. Husson, J. P. Chatry, and D. Michel, *J. Raman Spectrosc.* **14**, 63 (1983).
- ⁶⁸ S. P. S. Porto, P. A. Fleury, and T. C. Damen, *Phys. Rev.* **154**, 522 (1967).
- ⁶⁹ B. D. Gaulin, J. S. Gardner, S. R. Dunsiger, Z. Tun, M. D. Lumsden, R. F. Kiefl, N. P. Raju, J. N. Reimers, and J. E. Greedan, *Physica B* **241-243**, 511 (1998).
- ⁷⁰ M. Kanada, Y. Yasui, M. Ito, H. Harashina, M. Sato, H. Okumura, and K. Kakurai, *J. Phys. Soc. Japan* **68**, 3802 (1999).
- ⁷¹ S. W. Han, J. S. Gardner, and C. H. Booth, *Phys. Rev. B* **69**, 024416 (2004).
- ⁷² O. Ofer, A. Keren, and C. Baines, *J. Phys.: Condens. Matter* **19**, 145270 (2007).
- ⁷³ J. P. C. Ruff, B. D. Gaulin, J. P. Castellan, K. C. Rule, J. P. Clancy, J. Rodriguez, and H. A. Dabkowska, *Phys. Rev. Lett.* **99**, 237202 (2007).
- ⁷⁴ Y. M. Jana, A. Sengupta, and D. Ghosh, *J. Magn. Magn. Mater.* **248**, 7 (2002).
- ⁷⁵ S. Rosenkranz, A. P. Ramirez, A. Hayashi, R. J. Cava, R. Siddharthan, and B. S. Shastry, *J. Appl. Phys.* **87**, 5914 (2000).
- ⁷⁶ R. Siddharthan, B. S. Shastry, A. P. Ramirez, A. Hayashi, R. J. Cava, and S. Rosenkranz, *Phys. Rev. Lett.* **83**, 1854 (1999).
- ⁷⁷ Y. M. Jana and D. Ghosh, *Phys. Rev. B* **61**, 9657 (2000).

TABLE II: Experimentally determined and literature values of the frequencies (in cm^{-1}) of observed Raman modes in $\text{R}_2\text{Ti}_2\text{O}_7$ at room temperature and their respective symmetry assignments (between brackets).

R = Gd	This work			Saha <i>et al.</i> ⁵⁸	Zhang <i>et al.</i> ⁵⁹	Mori <i>et al.</i> ⁶⁰	Hess <i>et al.</i> ⁶¹	Gupta <i>et al.</i> ⁵⁷		Vandenborre <i>et al.</i> ⁶²
	Tb	Dy	Ho	Gd	Gd	Gd	Gd	Gd (<i>calcd.</i>)	Gd (<i>obs.</i>)	Gd
$\sim 104^a$	$\sim 102^a$	$\sim 103^a$	$\sim 105^a$ (-)	- (-)	- (-)	105 (F_{2g})	- (-)	- (-)	- (-)	110 (-)
$\sim 128^a$	-	$\sim 124^a$	$\sim 122^a$ (-)	- (-)	- (-)	125 (^b)	- (-)	- (-)	- (-)	215 (-)
205	209	212	214 (F_{2g})	215 (F_{2g})	210 (F_{2g})	222 (F_{2g})	219 (F_{2g})	230.6 (F_{2g})	225 (F_{2g})	225 (F_{2g})
260	256	269	297 (F_{2g})	- (-)	- (-)	- (-)	- (-)	- (-)	- (-)	- (-)
310	303	308	311 (F_{2g})	312 (F_{2g})	310 ^d (E_g)	311 (E_g)	312 (E_g)	318.0 (E_g)	- (-)	317 (F_{2g})
325	313	328	329 (E_g)	330 (E_g)	310 ^d (F_{2g})	- (-)	- (-)	328.2 (F_{2g})	317 (F_{2g})	347 ^e (E_g)
450 ^c	450 ^c	451 ^c	452 ^c (-)	- (-)	470 (F_{2g})	452 (-)	455 (F_{2g})	- (-)	- (-)	- (-)
-	-	-	- (-)	- (-)	- (-)	- (-)	- (-)	522.2 (F_{2g})	- (-)	- (-)
517	518	519	522 (A_{1g})	518 (A_{1g}/F_{2g})	520 (A_{1g})	518 (F_{2g})	519 (A_{1g})	526.8 (A_{1g})	515 (A_{1g})	515 ($A_{1g}+F_{2g}$)
554	557	550	562 (F_{2g})	547 (F_{2g})	570 (F_{2g})	585 (F_{2g})	549 (F_{2g})	594.0 (F_{2g})	580 (F_{2g})	580 (F_{2g})
$\sim 677^f$	$\sim 689^f$	$\sim 693^f$	$\sim 701^f$ (-)	684 (-)	- (-)	- (-)	680 (F_{2g})	- (-)	- (-)	- (-)
$\sim 703^f$	$\sim 706^f$	$\sim 720^f$	$\sim 724^f$ (-)	701 (-)	- (-)	- (-)	- (-)	- (-)	- (-)	705 (-)

^aThese modes are very weak and barely resolved, therefore their exact position is estimated.

^bMori *et al.* ascribe this band to trace amounts of Gd_2O_3 .

^cThis is a very weak mode, barely resolved above the noise. Mori *et al.* ascribe this mode to trace amounts of TiO_2 .

^dZhang *et al.* indicate the lower and higher wavenumber components of this band as the E_g and F_{2g} modes, respectively.

^eThis band has been calculated, rather than observed by Vandenborre *et al.*

^fThese overlapping modes comprise a weak band, in which the two modes cannot be separately resolved.